

# Renormalization group analysis of magnetic and superconducting instabilities near van Hove band fillings

A.A. Katanin<sup>a,b</sup> and A.P. Kampf<sup>a</sup>

<sup>a</sup> *Institut für Physik, Theoretische Physik III,*

*Elektronische Korrelationen und Magnetismus,*

*Universität Augsburg, 86135 Augsburg, Germany*

<sup>b</sup> *Institute of Metal Physics, 620219 Ekaterinburg, Russia*

## Abstract

Phase diagrams of the two-dimensional one-band  $t$ - $t'$  Hubbard model are obtained within the two-patch and the temperature-cutoff many-patch renormalization group approach. At small  $t'$  and at van Hove band fillings anti-ferromagnetism dominates, while with increasing  $t'$  or changing filling anti-ferromagnetism is replaced by  $d$ -wave superconductivity. Near  $t' = t/2$  and close to van Hove band fillings the system is unstable towards ferromagnetism. Away from van Hove band fillings this ferromagnetic instability is replaced by a region with dominating triplet  $p$ -wave superconducting correlations. The results of the renormalization-group approach are compared with the mean-field results and the results of the T-matrix approximation.

PACS numbers: 71.10.Fd; 71.27.+a; 74.25.Dw

## I. INTRODUCTION

The close relation between antiferromagnetism (AF) and  $d$ -wave superconductivity (dSC) was the subject of intensive investigations during the last two decades (see e.g. Refs. [1–5]). In particular, it was argued that the superconducting properties of high- $T_c$  (HTSC) materials are intimately related to their inherent antiferromagnetic correlations and many features of these materials were explained from the point of view of competition between antiferromagnetic and superconducting correlations [3]. On the other hand, AF spin fluctuations also serve as the natural candidate for the pairing mechanism of dSC [4,5]. A distinctly different physical situation is realized in the layered ruthenate  $\text{Sr}_2\text{RuO}_4$ , which is an unconventional and most likely triplet superconductor [6]. It was proposed, that the pairing in this material results from ferromagnetic spin fluctuations [7,8]. Although inelastic neutron scattering has so far been unsuccessful to detect significant low-energy ferromagnetic spin fluctuations in this material [9], this idea finds experimental support from the recent measurements of the susceptibility of the electron doped compound  $\text{Sr}_{2-x}\text{La}_x\text{RuO}_4$  [10] which revealed the tendency towards ferromagnetism with La doping. Furthermore, the isoelectronic compound  $\text{Ca}_2\text{RuO}_4$  also shows ferromagnetism under hydrostatic pressure [11].

Both, copper-oxide systems and  $\text{Sr}_2\text{RuO}_4$ , are layered materials. Therefore both systems motivate the investigation of the competition and the mutual interplay between magnetic and superconducting instabilities in two-dimensional (2D) correlated electron systems. For this type of analysis it is important to account for specific band structure related phenomena, namely for the form of the Fermi surface (FS) and the electronic dispersion. The influence of the shape of the FS on superconducting and magnetic properties is of interest from both, theoretical and experimental points of view and the theoretical analysis can be guided by material-specific information obtained from angle-resolved photoemission (ARPES) experiments [12–15].

The simplest theoretical model which allows to investigate the effect of the band dispersion on magnetic ordering and superconductivity of 2D systems is the single-band  $t$ - $t'$

Hubbard model on a square lattice which takes into account both nearest-neighbor  $t$  and next-nearest-neighbor  $t'$  hopping. This model is often discussed in connection with HTSC compounds, and it describes well the shape of the FSs of cuprate superconductors observed in ARPES [12–14]. In particular, the value  $t'/t = 0.15$  was chosen for  $\text{La}_2\text{CuO}_4$  and the value  $t'/t = 0.30$  for the Bi2212 system [16] in the tight-binding parametrization of the relevant electronic band for the  $\text{CuO}_2$ -planes, although the realistic modelling of the latter bilayer material requires the inclusion of interlayer hopping as well. On the other hand,  $\text{Sr}_2\text{RuO}_4$  has three relevant bands [17]. Interband effects are not negligible in this material, and may even prove important for the origin of unconventional superconductivity [18].

Already in early mean-field and quantum Monte Carlo (QMC) studies of the  $t$ - $t'$  Hubbard model [19] it was found that depending on the ratio  $t'/t$  and the band filling, different types of instabilities are possible. For small  $t'/t$  near half-filling the FS is almost nested, which is the origin for antiferromagnetism in the weak-coupling regime.  $t'$  hopping destroys the perfect nesting property of the FS and therefore leads to “frustration” of antiferromagnetism due to the hopping processes on the same sublattice and may therefore favor the emergence of a superconducting state [20]. Furthermore,  $t'$  hopping also weakens the tendency towards stripe formation [21] and by the suppression of this alternative instability superconducting fluctuations may get enhanced. At the same time, larger values of  $t'$  move the system closer to a ferromagnetic instability, since for  $t'/t$  close to  $1/2$  the dispersion is flattened close to the bottom of the band. This leads to flat-band ferromagnetism [22] at low densities which was investigated earlier for the  $2D$   $t$ - $t'$  Hubbard model within the  $T$ -matrix approximation [23,24] and projected QMC simulations [25].

The interplay of antiferromagnetism and  $d$ -wave superconductivity in the one-band  $t$ - $t'$  Hubbard model was recently reconsidered within many-patch renormalization-group (RG) approaches [26–28]. It was indeed verified that with increasing  $t'$  and/or decreasing band filling antiferromagnetism is replaced by  $d$ -wave superconductivity. In the early RG approaches of Refs. [26–28] particle-hole scattering at small momenta was not treated on equal footing with other types of scattering, and therefore these analyses were unable to search for a pos-

sible ferromagnetic instability (see the discussion in Refs. [29,30]). It was shown in Ref. [31] however, that particle-hole scattering at small momenta does indeed lead to the appearance of a ferromagnetic phase at large enough  $t'/t$  and at van Hove (vH) band fillings; the onset of dominant ferromagnetic correlations was found to occur for  $t'/t > 0.27$ . However, unlike in Refs. [26–28], the contribution of the Cooper channel was not taken into account in Ref. [31]. The possibility of a ferromagnetic instability was also investigated within a simplified two-patch RG scheme [29], which considers only the scattering of electrons in the vicinity of the “singular” points  $(\pi, 0)$  and  $(0, \pi)$  in momentum space and therefore gives only a rough picture for the RG scaling behavior of the coupling constants. The temperature-cutoff version of the many-patch RG approach (TCRG) recently introduced by Honerkamp and Salmhofer [30] includes the contributions of the whole Brillouin zone and uses the temperature as a natural low-energy cutoff parameter in order to avoid the technical difficulties with the inclusion of small-momentum particle-hole scattering. It was demonstrated in Refs. [29,30] that the proper account of all scattering channels indeed leads to ferromagnetism at large enough  $t'/t$ . Moreover, the critical value of  $(t'/t)_c$  for the stability of ferromagnetism is  $U$ -dependent [29] (unlike the results of Ref. [31]), in particular for  $U \rightarrow 0$  ferromagnetism exists only in the flat-band low-density limit  $(t'/t)_c \rightarrow 1/2$  in qualitative agreement with the results of the  $T$ -matrix approximation for the effective electron-electron interaction vertex [23]. Naturally, ferromagnetic and  $d$ -wave superconducting fluctuations tend to suppress each other [29,30]. The suppression of ferromagnetism by superconducting fluctuations is reminiscent of the well-known Kanamori screening [32]. On the other hand, as shown in Ref. [30], the tendency towards *triplet* superconductivity is enhanced by ferromagnetic fluctuations and may exist in the vicinity of a ferromagnetic phase. Note that the Pomeranchuk instability, which was proposed for small  $t'$  in Ref. [33], was shown to be a non-leading instability in the  $t$ - $t'$  Hubbard model [34].

With these recent results it appears as a natural task to investigate systematically the weak-coupling phase diagram of the 2D Hubbard model within the RG approach. Earlier, such an analysis was performed only with the momentum cutoff RG versions [26–28], which,

as we discussed above, do not allow to include the contribution of ferromagnetic fluctuations. Previous studies of the model with the inclusion of all electron scattering channels were performed either in the two-patch RG scheme [29], which is restricted to vH band fillings or within the TCRG approach [30,34], which however was applied only for some selected parameter values and therefore results for a phase diagram in the weak-coupling regime were not obtained.

The purpose of the present paper is to investigate systematically different types of instabilities of the  $t$ - $t'$  Hubbard model within two-patch and the many-patch TCRG approach. The paper is organized as follows. In Section II we give a summary of the RG methods we use. In Section III we present the phase diagrams obtained and compare the results with previous investigations of the  $t - t'$  Hubbard model. In Section IV we discuss the results and conclude.

## II. RENORMALIZATION-GROUP APPROACHES

We consider the  $t$ - $t'$  Hubbard model

$$H = - \sum_{ij\sigma} t_{ij} c_{i\sigma}^\dagger c_{j\sigma} + U \sum_i n_{i\uparrow} n_{i\downarrow} - (\mu - 4t')N \quad (1)$$

where the hopping amplitude  $t_{ij} = t$  for nearest neighbor sites  $i$  and  $j$  and  $t_{ij} = -t'$  for next-nearest neighbor sites ( $t, t' > 0$ ) on a square lattice (we have shifted the chemical potential  $\mu$  by  $4t'$  for further convenience). In momentum space Eq. (1) reads

$$H = \sum_{\mathbf{k}\sigma} \varepsilon_{\mathbf{k}} c_{\mathbf{k}\sigma}^\dagger c_{\mathbf{k}\sigma} + \frac{U}{2N^2} \sum_{\mathbf{k}_1\mathbf{k}_2\mathbf{k}_3\mathbf{k}_4} \sum_{\sigma\sigma'} c_{\mathbf{k}_1\sigma}^\dagger c_{\mathbf{k}_2\sigma'}^\dagger c_{\mathbf{k}_3\sigma'} c_{\mathbf{k}_4\sigma} \delta_{\mathbf{k}_1+\mathbf{k}_2-\mathbf{k}_3-\mathbf{k}_4} \quad (2)$$

where the Kronecker  $\delta$ -symbol ensures momentum conservation and the dispersion has the form

$$\varepsilon_{\mathbf{k}} = -2t(\cos k_x + \cos k_y) + 4t'(\cos k_x \cos k_y + 1) - \mu \quad (3)$$

where the lattice constant is set to unity. The tight-binding spectrum (3) leads to vH singularities (vHS) in the density of states arising from the contributions around the points

$\mathbf{k}_A = (\pi, 0)$  and  $\mathbf{k}_B = (0, \pi)$ . These singularities lie at the FS if  $\mu = 0$ . For  $t' = 0$  the corresponding filling is  $n_{vH} = 1$  and the FS is nested, but the nesting is removed for any  $t' \neq 0$ . The dependence of the vH band filling on  $t'$  is shown in Fig.1, and the shape of the FS at different  $t'/t$  and vH band fillings is shown in Fig. 2.

The standard RG strategy for fermion systems [35] is to integrate out step by step the electronic states which are far from the FS (i.e. the states with the energy  $\Lambda - d\Lambda < \varepsilon_{\mathbf{k}} < \Lambda$  at each RG step). This procedure meets a difficulty when it is applied to a FS with singular points, i.e. the points  $\mathbf{k}_F^s$  with vanishing Fermi velocity  $\nabla \varepsilon_{\mathbf{k}}|_{\mathbf{k}=\mathbf{k}_F^s} = \mathbf{0}$ , as in points  $\mathbf{k}_A$  and  $\mathbf{k}_B$ . In this case, the states with the same excitation energy  $\varepsilon_{\mathbf{k}}$  become inequivalent: the excitations with momenta closer to the singular points produce more divergent contributions to the renormalization of the electron-electron interaction vertices than the excitations with momenta far from the singular points. Therefore, an additional separation of the momenta besides the standard separation into “slow” ( $\varepsilon_{\mathbf{k}} < \Lambda$ ) and “fast” ( $\varepsilon_{\mathbf{k}} > \Lambda$ ) modes is needed. The two-patch approach which we consider in Sect. IIIa accounts only for the most singular contributions coming from the immediate vicinities of the singular points. The more sophisticated many-patch approaches of Refs. [26–28,30] (see Sect. IIIb) take into account the momentum dependence of the interaction in a more accurate way by introducing a set of patches which cover the entire Brillouin zone and parametrize the interactions by the position of incoming and outgoing momenta on the patched FS.

### A. Two-patch renormalization-group approach

The two-patch approach [36,37,29] is restricted to the vH band fillings only. At these fillings the density of states at the Fermi energy and the electron-electron interaction vertices at momenta  $\mathbf{k}_i = \mathbf{k}_{A,B}$  contain logarithmic divergencies arising from the momentum integrations in the vicinity of the points  $\mathbf{k}_{A,B}$ . Therefore these contributions are the most important for the calculation of the renormalized interaction vertices. Accordingly, we subdivide the momentum space into three types of regions (see Fig. 3). Regions I with  $\mathbf{k} \in O(A) \vee O(B)$

where

$$O(A) = \{\mathbf{k} : |\mathbf{k} - \mathbf{k}_A| < \Lambda \wedge |\varepsilon_{\mathbf{k}}/t| > e^{-\Lambda/|\mathbf{k}-\mathbf{k}_A|}\} \quad (4)$$

and similar for  $O(B)$  ( $\Lambda$  is a momentum cutoff parameter) produce the most singular contribution to the renormalization of the vertices. Regions II contain the electronic states which are close to the FS but far from vH singularities. It can be proven that the contributions of regions II to the renormalization of the vertices is subleading in comparison with the contributions of regions I, provided that  $t'/t$  is not small, i.e. if the nesting effects are not important. Finally, regions III contain the excitations which are far from both, the FS and vHS and do not produce diverging contributions to any quantity. Therefore, in the simplest approximation it is reasonable to neglect the contributions of regions II and III altogether. A more accurate treatment within the many-patch RG approach will be performed in the next section.

To account for the excitations with momenta in regions I, it is convenient to introduce new electron operators  $a_{\mathbf{k}}$  and  $b_{\mathbf{k}}$  by

$$c_{\mathbf{k}\sigma} = \begin{cases} a_{\mathbf{k}-\mathbf{k}_A,\sigma} & \mathbf{k} \in O(A) \\ b_{\mathbf{k}-\mathbf{k}_B,\sigma} & \mathbf{k} \in O(B) \end{cases}.$$

For momenta  $\mathbf{k} \in O(A) \vee O(B)$  in the vicinity of the vH points the dispersion is expanded as

$$\varepsilon_{\mathbf{k}_A+\mathbf{p}} \equiv \varepsilon_{\mathbf{p}}^A = -2t(\sin^2 \varphi p_x^2 - \cos^2 \varphi p_y^2) - \mu \quad (5a)$$

$$= -2tp_+p_- - \mu$$

$$\varepsilon_{\mathbf{k}_B+\mathbf{p}} \equiv \varepsilon_{\mathbf{p}}^B = 2t(\cos^2 \varphi p_x^2 - \sin^2 \varphi p_y^2) - \mu \quad (5b)$$

$$= 2t\tilde{p}_+\tilde{p}_- - \mu$$

where  $\cos(2\varphi) = R = 2t'/t$ ,  $p_{\pm} = p_x \sin \varphi \pm p_y \cos \varphi$ , and  $\tilde{p}_{\pm} = p_x \cos \varphi \pm p_y \sin \varphi$ . Using the new electron operators we write the effective Hamiltonian in the form

$$H = \sum_{\mathbf{p}\sigma} \varepsilon_{\mathbf{p}}^A a_{\mathbf{p}\sigma}^\dagger a_{\mathbf{p}\sigma} + \sum_{\mathbf{p}\sigma} \varepsilon_{\mathbf{p}}^B b_{\mathbf{p}\sigma}^\dagger b_{\mathbf{p}\sigma}$$

$$\begin{aligned}
& + \frac{2\pi^2 t}{N^2} \sum_{\mathbf{p}_i, \sigma \sigma'} [g_1(\lambda) a_{\mathbf{p}_1 \sigma}^\dagger b_{\mathbf{p}_2 \sigma'}^\dagger a_{\mathbf{p}_3 \sigma'} b_{\mathbf{p}_4 \sigma} + g_2(\lambda) a_{\mathbf{p}_1 \sigma}^\dagger b_{\mathbf{p}_2 \sigma'}^\dagger b_{\mathbf{p}_3 \sigma'} a_{\mathbf{p}_4 \sigma}] \delta_{\mathbf{p}_1 + \mathbf{p}_2 - \mathbf{p}_3 - \mathbf{p}_4} \\
& + \frac{\pi^2 t}{N^2} \sum_{\mathbf{p}_i, \sigma \sigma'} [g_3(\lambda) a_{\mathbf{p}_1 \sigma}^\dagger a_{\mathbf{p}_2 \sigma'}^\dagger b_{\mathbf{p}_3 \sigma'} b_{\mathbf{p}_4 \sigma} + g_4(\lambda) a_{\mathbf{p}_1 \sigma}^\dagger a_{\mathbf{p}_2 \sigma'}^\dagger a_{\mathbf{p}_3 \sigma'} a_{\mathbf{p}_4 \sigma} + a \leftrightarrow b] \delta_{\mathbf{p}_1 + \mathbf{p}_2 - \mathbf{p}_3 - \mathbf{p}_4} \quad (6)
\end{aligned}$$

where

$$\lambda = \ln(\Lambda / \max(p_{i+}, p_{i-}, \tilde{p}_{i+}, \tilde{p}_{i-}, T/t)); \quad (7)$$

the summation in Eq. (6) is restricted to momenta  $\mathbf{p}_i$  with  $|\mathbf{p}_i| < \Lambda$  and  $|\varepsilon_{\mathbf{k}_{A,B} + \mathbf{p}_i}/t| > e^{-\Lambda/|\mathbf{p}_i|}$ .

As shown in Fig. 4, the vertices  $g_1$  to  $g_4$  represent different types of scattering processes of electrons with momenta close to the vHS. The bare value for all four vertices is  $g_i^0 = U/(4\pi^2 t)$ . The momentum dependence of the vertex inside regions I is accounted for through the scaling variable  $\lambda$  only. Note however, that the momentum dependence of the electronic spectrum within each patch is correctly taken into account in the two-patch approach.

To obtain the dependence of the vertices  $g_i$  on  $\lambda$  we integrate out at each RG step the fermions  $a_{\mathbf{p}}$  with momenta  $\Lambda e^{-\lambda} < p_{\pm} < \Lambda e^{-\lambda-d\lambda}$ , and fermions  $b_{\mathbf{p}}$  with momenta  $\Lambda e^{-\lambda} < \tilde{p}_{\pm} < \Lambda e^{-\lambda-d\lambda}$  (see the detailed description in Ref. [38]). As argued above we neglect the renormalization of the  $g_i$  arising from the regions II and III of Fig. 3 since this leads to subleading corrections at weak coupling. We determine the RG equations for the vertices  $g_i(\lambda)$  in the form [36–38,29]

$$\begin{aligned}
dg_1/d\lambda &= 2d_1(\lambda)g_1(g_2 - g_1) + 2d_2g_1g_4 - 2d_3g_1g_2, \\
dg_2/d\lambda &= d_1(\lambda)(g_2^2 + g_3^2) + 2d_2(g_1 - g_2)g_4 - d_3(g_1^2 + g_2^2), \\
dg_3/d\lambda &= -2d_0(\lambda)g_3g_4 + 2d_1(\lambda)g_3(2g_2 - g_1), \\
dg_4/d\lambda &= -d_0(\lambda)(g_3^2 + g_4^2) + d_2(g_1^2 + 2g_1g_2 - 2g_2^2 + g_4^2), \quad (8)
\end{aligned}$$

where

$$\begin{aligned}
d_0(\lambda) &= 2\lambda/\sqrt{1-R^2}, \quad d_2 = 2/\sqrt{1-R^2}; \\
d_3 &= 2 \tan^{-1}(R/\sqrt{1-R^2})/R; \\
d_1(\lambda) &= 2 \min\{\lambda, \ln[(1 + \sqrt{1-R^2})/R]\}. \quad (9)
\end{aligned}$$



Eqs. (8) have to be solved with the initial conditions  $g_i(0) = g_i^0$ .

The authors of Ref. [31] argued that the kinematic restrictions lead to the absence of particle-particle scattering contributions to the vertices  $g_i$  ( $d_0 = d_3 = 0$  in our notations). This conclusion however is connected with the difficulty of the infinitesimal version of Wilson's RG approach with a sharp momentum cutoff, since this approach does not allow to treat correctly the vertices with nonzero momentum transfer and gives artificially no renormalization for such vertices [39]. That is why in the present approach we consider the vertices at the special vH points only, rather than considering vertices with arbitrary momentum transfers. Note that this difficulty does not arise in Wilson's RG approach with a smooth cutoff and/or discrete RG transformations [39]; in this case particle-particle scattering does contribute to the renormalization of the vertices with arbitrary momenta.

In order to explore the possible instabilities of the system, we consider the behavior of the zero-frequency, time-ordered response functions

$$\chi_m = \int_0^{1/T} d\tau \langle \mathcal{T} [\hat{O}_m^\dagger(\tau) \hat{O}_m(0)] \rangle \quad (10)$$

in the zero-temperature limit  $T \rightarrow 0$ .  $\hat{O}_m(\tau)$  are the following operators

$$\begin{aligned} \hat{O}_{\text{AF}} &= \frac{1}{N} \sum_{\mathbf{k}} \sigma c_{\mathbf{k},\sigma}^\dagger c_{\mathbf{k}+\mathbf{Q},\sigma}, \\ \hat{O}_{\text{dSC}} &= \frac{1}{N} \sum_{\mathbf{k}\sigma} f_{\mathbf{k}} \sigma c_{\mathbf{k},\sigma}^\dagger c_{-\mathbf{k},-\sigma}^\dagger, \\ \hat{O}_{\text{F}} &= \frac{1}{N} \sum_{\mathbf{k}\sigma} \sigma c_{\mathbf{k},\sigma}^\dagger c_{\mathbf{k},\sigma}, \end{aligned} \quad (11)$$

in the Heisenberg representation,  $\mathcal{T}$  is the imaginary time ordering operation, and  $\mathbf{Q} = (\pi, \pi)$ . The order parameters which correspond to  $p$ -wave pairing

$$\hat{O}_{\text{pSC}}^{x,y} = \frac{1}{N} \sum_{\mathbf{k}\sigma} h_{\mathbf{k}}^{x,y} c_{\mathbf{k},\sigma}^\dagger c_{-\mathbf{k},-\sigma}^\dagger, \quad (12)$$

with  $h_{\mathbf{k}}^{x,y} = \sin k_{x,y}$  are irrelevant with the restriction of momenta to the vicinities of vH points, since  $h_{\mathbf{k}_{A,B}} = 0$  and therefore the possibility of triplet pairing can not be considered

within the two-patch approach. However, these order parameters can be taken into account in many-patch approaches (see Section IIIb).

Picking up the logarithmical divergences in  $\lambda$  we obtain the RG equations for the dimensionless susceptibilities  $\bar{\chi}_m = 2\pi^2 t \chi_m$  in the same approximations as discussed above (cf. Refs. [36,37,29]):

$$\begin{aligned} d\bar{\chi}_m(\lambda)/d\lambda &= d_{a_m}(\lambda)\mathcal{R}_m^2(\lambda), \\ d\ln \mathcal{R}_m(\lambda)/d\lambda &= d_{a_m}(\lambda)\Gamma_m(\lambda), \end{aligned} \tag{13}$$

where the coefficients  $\Gamma_m$  ( $m = \text{AF, dSC, or F}$ ) are given by

$$\begin{aligned} \Gamma_{\text{AF}} &= g_2 + g_3; \quad \Gamma_{\text{F}} = g_1 + g_4; \\ \Gamma_{\text{dSC}} &= g_3 - g_4. \end{aligned} \tag{14}$$

In Eqs. (13)  $a_{\text{dSC}} = 0$ ,  $a_{\text{AF}} = 1$ , and  $a_{\text{F}} = 2$ . Eqs. (13) have to be solved with the initial conditions  $\mathcal{R}_m(0) = 1$ ,  $\chi_m(0) = 0$ .

The numerical solutions of Eqs. (8) show, that at a critical value  $\lambda_c$  of the scaling parameter  $\lambda$  some of the vertices and susceptibilities are divergent. For a given  $\lambda_c$  the size  $\Lambda$  of the patches is restricted by  $\ln(4/\Lambda) \ll \lambda_c$ . The latter criterion follows from the condition that the contribution of the electrons with  $|k_{\pm}| < \Lambda$  to particle-hole and particle-particle bubbles is dominant (see e.g. Ref. [40]). We choose  $\Lambda = 1$  and require  $\lambda_c \gg \ln 4 \simeq 1$ . Since  $\lambda_c$  decreases with increasing interaction strength, this criterion defines the interaction range where the two-patch RG approach is valid.

As an example, we show in Figs. 5,6 the result of the numerical solutions of Eqs. (8) for  $U = 2t$  and two different choices of  $t'/t = 0.1$  and  $t'/t = 0.45$ . The behavior of the coupling constants is qualitatively different in these two cases. While in the first case we have  $g_{2,3}$  flowing to  $+\infty$ ,  $g_4$  to  $-\infty$ , and  $g_1$  is mostly unchanged during the RG flow (we denote the corresponding combination  $(m++)$ , the signs correspond to the behavior of the coupling constants  $g_1$ - $g_4$ ,  $m$  means marginal. In the second case  $g_{1,2,4}$  grow to  $+\infty$  while  $g_3$  goes to zero, i.e. we observe  $(++0+)$  behavior of the coupling constants. The comparison of the

corresponding susceptibilities shows that for  $t'/t = 0.1$  the antiferromagnetic susceptibility is the most divergent, while in the case  $t'/t = 0.45$  the ferromagnetic susceptibility dominates and therefore the two different coupling constant flows reflect two different instabilities of the system. We discuss the complete phase diagram at vH band fillings in Sect. IIIa.

## B. Many-patch renormalization-group analysis

In the many-patch analysis we follow the temperature-cutoff RG for one-particle irreducible Green functions proposed recently by Honerkamp and Salmhofer in Ref. [30]. This version of the RG uses the temperature as a natural cutoff parameter, allowing to account for both the excitations with momenta close to the FS and far from it, which is necessary for the description of instabilities which arise from zero-momentum particle-hole scattering, e.g. ferromagnetism. Neglecting the frequency dependence of the vertices, which is considered not important in the weak-coupling regime, the RG differential equation for the temperature- and momentum-dependent electron-electron interaction vertex has the form [30] (see Fig. 7)

$$\begin{aligned} \frac{d}{dT} V_T(\mathbf{k}_1, \mathbf{k}_2, \mathbf{k}_3) = & -\frac{1}{N} \sum_{\mathbf{p}} V_T(\mathbf{k}_1, \mathbf{k}_2, \mathbf{p}) L_{\text{pp}}(\mathbf{p}, -\mathbf{p} + \mathbf{k}_1 + \mathbf{k}_2) V_T(\mathbf{p}, -\mathbf{p} + \mathbf{k}_1 + \mathbf{k}_2, \mathbf{k}_3) \\ & + \frac{1}{N} \sum_{\mathbf{p}} [-2V_T(\mathbf{k}_1, \mathbf{p}, \mathbf{k}_3) V_T(\mathbf{p} + \mathbf{k}_1 - \mathbf{k}_3, \mathbf{k}_2, \mathbf{p}) + V_T(\mathbf{k}_1, \mathbf{p}, \mathbf{k}_3) V_T(\mathbf{k}_2, \mathbf{p} + \mathbf{k}_1 - \mathbf{k}_3, \mathbf{p}) \\ & + V_T(\mathbf{k}_1, \mathbf{p}, \mathbf{p} + \mathbf{k}_1 - \mathbf{k}_3) V_T(\mathbf{p} + \mathbf{k}_1 - \mathbf{k}_3, \mathbf{k}_2, \mathbf{p})] L_{\text{ph}}(\mathbf{p}, \mathbf{p} + \mathbf{k}_1 - \mathbf{k}_3) \\ & + \sum_{\mathbf{p}} V_T(\mathbf{k}_1, \mathbf{p} + \mathbf{k}_2 - \mathbf{k}_3, \mathbf{p}) L_{\text{ph}}(\mathbf{p}, \mathbf{p} + \mathbf{k}_2 - \mathbf{k}_3) V_T(\mathbf{p}, \mathbf{k}_2, \mathbf{k}_3) \end{aligned} \quad (15)$$

where

$$\begin{aligned} L_{\text{ph}}(\mathbf{k}, \mathbf{k}') &= \frac{f'_T(\varepsilon_{\mathbf{k}}) - f'_T(\varepsilon_{\mathbf{k}'})}{\varepsilon_{\mathbf{k}} - \varepsilon_{\mathbf{k}'}} , \\ L_{\text{pp}}(\mathbf{k}, \mathbf{k}') &= \frac{f'_T(\varepsilon_{\mathbf{k}}) + f'_T(\varepsilon_{\mathbf{k}'})}{\varepsilon_{\mathbf{k}} + \varepsilon_{\mathbf{k}'}} , \end{aligned} \quad (16)$$

and  $f'_T(\varepsilon) = df(\varepsilon)/dT$ ,  $f(\varepsilon)$  is the Fermi function. Eq. (15) has to be solved with the initial condition  $V_{T_0}(\mathbf{k}_1, \mathbf{k}_2, \mathbf{k}_3) = U$  where the initial temperature  $T_0$  is of the order of the bandwidth.

The evolution of the vertices with decreasing temperature determines the temperature dependence of the susceptibilities according to [30,34]

$$\begin{aligned}\frac{d}{dT}\chi_{mT} &= \sum_{\mathbf{k}'} \mathcal{R}_{mT}(\mathbf{k}') \mathcal{R}_{mT}(\mp \mathbf{k}' + \mathbf{q}_m) L_{pp,ph}(\mathbf{k}', \mp \mathbf{k}' + \mathbf{q}_m), \\ \frac{d}{dT}\mathcal{R}_{mT}(\mathbf{k}) &= \mp \sum_{\mathbf{k}'} \mathcal{R}_{mT}(\mathbf{k}') \Gamma_{mT}(\mathbf{k}, \mathbf{k}') L_{pp,ph}(\mathbf{k}', \mp \mathbf{k}' + \mathbf{q}_m)\end{aligned}\tag{17}$$

where

$$\Gamma_{mT}(\mathbf{k}, \mathbf{k}') = \begin{cases} V_T(\mathbf{k}, \mathbf{k}', \mathbf{k}' + \mathbf{q}_m) & \text{for } m = \text{AF or F} \\ V_T(\mathbf{k}, -\mathbf{k}, \mathbf{k}') & \text{for } m = \text{dSC or pSC} \end{cases}.\tag{18}$$

$\mathbf{q}_m = \mathbf{Q}$  for the AF susceptibility and  $\mathbf{q}_m = \mathbf{0}$  otherwise. The upper signs and *pp* indices in Eq. (17) refer to the superconducting instabilities (dSC and pSC), and the lower signs and *ph* indices to the other susceptibilities. The initial conditions for Eqs. (17) are

$$\mathcal{R}_{m,T_0}(\mathbf{k}) = \begin{cases} \cos k_x - \cos k_y & \text{for dSC} \\ \sin k_{x,y} & \text{for pSC} \\ 1 & \text{otherwise} \end{cases},\tag{19}$$

and  $\chi_{m,T_0} = 0$ . To solve numerically Eqs. (15) and (17), we use the discretization of momentum space in  $N_p = 48$  patches and the same patching scheme as proposed in Ref. [30]. By exploiting the symmetries of the square lattice, this reduces the above integro-differential equations (15) and (17) to a set of 5824 differential equations which were solved numerically. We use the value of the starting temperature  $T_0 = 12t$ , which is slightly larger than the bandwidth, and we stop the flow of the coupling constants at the temperature  $T_X$  when the maximum absolute value of the vertex function is larger than  $V_{\max} = 18t$ . Note that the initial  $\mathbf{k}$ -dependence of the vertices (19) is slightly changed during the RG flow: the vertices which correspond to *d*- and *p*-wave superconductivity acquire *g*- and *f*-wave (and even higher order) harmonics, respectively, and the vertices which have *s*-wave symmetry (F, AF) acquire an additional extended *s*-wave ( $\cos k_x + \cos k_y$ ) component. However, these additional corrections are small.

To extract more detailed information about different instabilities we extrapolate the inverse susceptibilities  $\chi_{mT}^{-1}$  to temperatures lower than  $T_X$ . For magnetically ordered or superconducting ground states the corresponding extrapolated inverse susceptibilities  $\chi_{mT}^{-1}$  vanish at some temperature  $T_m^*$  below  $T_X$ . The vanishing of the inverse susceptibilities at finite temperatures is an artifact of the one-loop RG approach and should be understood to determine a crossover temperature into a renormalized classical regime with strong magnetic or superconducting fluctuations and exponentially large correlation length  $\xi \propto \exp(A/T)$  for F and AF instabilities (see Appendix) and  $\xi \propto \exp(A/\sqrt{T - T_{\text{BKT}}})$  for superconducting instabilities.  $T_{\text{BKT}}$  is the Berezinskii-Kosterlitz-Thouless transition temperature which arises because the superconducting transition in 2D is in the same symmetry class as the classical 2D XY model [44,45]. Although the inverse magnetic susceptibilities must be finite at  $T < T_{\text{F,AF}}^*$ , they are exponentially small, since in this regime  $\chi_{\text{F,AF}}^{-1} \propto \xi^{-2}$ , cf. Refs. [41–43]. The same concerns the superconducting susceptibilities in the temperature range  $T_{\text{BKT}} < T < T_{\text{dSC,pSC}}^*$ , where critical behavior  $\chi_{\text{dSC,pSC}}^{-1} \propto \xi^{-2+\eta}$  ( $\eta \cong 1/4$  is the critical exponent for the susceptibility) as for the XY model [44] is expected. At  $T < T_{\text{BKT}}$  the superconducting correlations have power law decay in real space and the inverse static uniform order parameter susceptibility does indeed vanish.

### III. RESULTS AND PHASE DIAGRAMS

#### A. van Hove band fillings

First we trace the vH band fillings at different  $t'$ , which are determined by the condition  $\mu = 0$ . The corresponding phase diagram in  $t' - U$  coordinates is plotted in Fig. 8. Solid lines correspond to the phase boundaries obtained within the two-patch approach, while the symbols show different types of instabilities obtained within the many-patch RG scheme [46]. Our many-patch results for  $U = 3t$  agree quantitatively with those obtained previously in Ref. [30].

In both approaches we find antiferromagnetism for small  $t'$ , ferromagnetism for  $t'$  close to  $1/2$  and  $d$ -wave superconductivity for intermediate  $t'$ . The  $t'$  range with a tendency towards  $d$ SC decreases with increasing  $U$ . For intermediate  $t'/t$  the susceptibilities with momenta  $\mathbf{Q}=(\pi-\delta, \pi)$  are stronger than the antiferromagnetic susceptibility. The incommensurate magnetic regions are indicated in Fig. 8 as well. In the region  $t'/t \sim 0.3$  the behavior of the coupling constants in the two-patch approach becomes “frustrated”, namely all  $g_i \rightarrow 0$  with increasing  $\lambda$ . This frustration is the consequence of the competition of antiferromagnetic and superconducting instabilities from one side and the ferromagnetic instability from the other side and therefore at  $t'/t > 0.2$  neither the antiferromagnetic nor the superconducting susceptibility diverges in the two-patch approach. The many-patch approach suffers less from this problem; the frustrated behavior of the vertices is observed only very close to the boundary of ferromagnetic and antiferromagnetic or superconducting phases.

The boundary to the ferromagnetic phase appears almost identical in two- and many-patch approaches, but the two-patch approach fails to reproduce the location of the phase boundary between the antiferromagnetic and superconducting phases for small  $t'$ . This is similar to the results for the extended  $U$ - $V$ - $J$  Hubbard model [38]. As mentioned in Section IIa, this difference is traced to the same behavior  $(m++-)$  of the coupling constants on approaching AF and dSC instabilities, while the ferromagnetic phase is signalled by a different behavior of the coupling constants  $(++0+)$ . Furthermore, the near-nesting effects, which are not accounted for in the two-patch RG approach become particularly important at small  $t'/t$ .

We also mark in Fig. 8 the result of Alvarez et al. [31] for the boundary of the ferromagnetic phase, obtained by neglecting the contribution of particle-particle scattering. In this case the corresponding two-patch RG equations can be solved analytically, since the coefficients  $d_i$  in Eq. (8) become  $\lambda$ -independent. The main difference in comparison with Ref. [31] is that particle-particle scattering leads to a  $U$ -dependence of the critical value  $(t'/t)_c$  for the appearance of ferromagnetism so that  $(t'/t)_c \rightarrow 1/2$  for  $U \rightarrow 0$  in qualitative agreement with the results of the  $T$ -matrix approximation [23]. At the same time, neglect-

ing particle-particle scattering gives  $(t'/t)_c \simeq 0.27$  independent of  $U$ . Note that the value  $(t'/t)_c$  is determined by the condition of equal non-interacting particle-hole susceptibilities  $\chi_0(\mathbf{0}) = \chi_0(\mathbf{Q})$  and therefore coincides with the “mean-field” criterion for the boundary of the ferromagnetic phase.

### B. Antiferromagnetic instability at small $t'$

The case  $t' = 0$  for fillings close to  $n = 1$  was intensively studied previously within momentum-cutoff RG approaches [26,27]. We plot the results of TCRG at  $t' = 0$  in Fig. 9. There is a line of critical concentrations  $n_c(U)$  such that for  $n < n_c(U)$  the extrapolated inverse susceptibility  $\chi_{\text{AF}}^{-1}$  does not reach zero for any temperature and the ground state is expected not to have long-range antiferromagnetic order. For comparison, we also plot the result for the critical concentrations obtained within the momentum-cutoff RG approach, Ref. [27]. Both approaches give practically indistinguishable results for the critical fillings where antiferromagnetism disappears. Mean-field theory predicts a broader concentration range for the stability of antiferromagnetism, see Fig. 9. It was proven by van Dongen [47] that for large space dimensionality  $d \gg 1$  and  $U \ll t$  the critical hole concentration  $\delta_c = 1 - n_c$  is reduced in comparison with its mean-field value  $\delta_c^{\text{MF}}$  by a *finite* factor  $q_d$ . To analyze whether this remains true for  $d = 2$  we consider the  $U$ -dependence of the ratio  $q(U) = \delta_c/\delta_c^{\text{MF}}$ . We find that  $q(U)$  slightly decreases with decreasing  $U$  and it is saturating at  $q(0) \simeq 0.4 \pm 0.025$ . Surprisingly, the formal application of the results of  $1/d$  expansion in Ref. [47] to  $d = 2$  gives a close value,  $q_2 = 0.3$ .

We have verified that within the antiferromagnetic phase at  $t' = 0$  the susceptibilities at wavevectors  $\mathbf{Q} \neq (\pi, \pi)$  are always smaller than the susceptibility  $\chi_{\text{AF}}$ , so that the tendency towards incommensurate magnetic order is subleading in comparison with commensurate  $(\pi, \pi)$  order. The fact that we identify commensurate AF even away from half filling may be reconciled with the possibility that the system develops inhomogeneous spin and charge structures (e.g. phase separation), as was obtained in the mean-field studies of the Hubbard

model [48] and the weak-coupling results in high dimensions [47].

Outside the antiferromagnetic region we find the tendency towards  $d$ SC as observed previously in Refs. [27,34]. The values of the crossover temperature  $T_{\text{dSC}}^*$  rapidly decrease away from the antiferromagnetic phase; we show in Fig. 9 the contour lines with  $\ln(t/T_{\text{dSC}}^*) = 5, 6, 7$ . The contour lines with larger  $T_{\text{dSC}}^*$  can not be traced within the present RG analysis: because of strong fluctuations near the AF phase, the coupling constants reach  $V_{\text{max}} = 18t$  before the  $d$ -wave susceptibility becomes large. On the other hand, smaller  $T_{\text{dSC}}^*$  (and correspondingly larger deviations from half filling) are hard to treat, too, because of the difficulties with the numerical integrations in Eqs. (15) since the integrands contain sharp Fermi functions at small temperatures.

The half-filled case at different  $t'$  was investigated previously within a mean-field analysis [49–51], QMC calculations [19,50], and path-integral RG [52]. Different methods predict different values of the critical interaction  $U_c$  for the onset of antiferromagnetism at fixed  $t'$ . In particular for  $t'/t = 0.2$  QMC results on an  $8 \times 8$  lattice [19,50] at  $T = 0.25t$  yield  $U_c = 2.5t$ , while path-integral RG [52] gives  $U_c = 3.4t$ . The result of the mean-field approach for the same  $t'/t$  is  $U_c = 2t$  [49–51]. We present our phase diagram as obtained from the many-patch RG analysis in Fig. 10; symbols show the critical values  $U_c$  obtained by other methods. As expected and in agreement with previous studies, the critical  $U_c$  is larger than the mean-field value for all  $t'$ . At the same time, the  $U_c$  result of the TCRG at  $t'/t = 0.2$  is larger than that from QMC calculations, but it agrees well with the path-integral RG result in Ref. [52].

Again, we find the tendency towards  $d$ SC away from the AF region; we show in Fig. 10 the contour lines which correspond to  $\ln(t/T_{\text{dSC}}^*) = 5, 6, 7$ . Note that from the extrapolation of these data to larger  $U$  in the paramagnetic phase ( $U < U_c$ ) we always find  $\ln(t/T_{\text{dSC}}^*) > 3$  in the weak-coupling regime, i.e. a temperature regime which is far below the accessible temperature range in QMC simulations. Therefore, it may be difficult if not impossible to observe the corresponding superconducting fluctuations in QMC calculations on finite lattice sizes - at least in the weak-to intermediate coupling regime.



### C. Ferromagnetic instability

Now we investigate the ferromagnetic instability, which arises for  $t'/t$  close to  $1/2$ . We start with  $t'/t = 1/2$ , when the dispersion at the bottom of the band at small  $k_x$  or  $k_y$  can be expanded as

$$\varepsilon_{\mathbf{k}} = \begin{cases} tk_x^2(1 - \cos k_y) - \mu, & k_x \ll 1 \\ tk_y^2(1 - \cos k_x) - \mu, & k_y \ll 1 \end{cases}, \quad (20)$$

i.e. it has extended minima along the lines  $k_x = 0$  and  $k_y = 0$  (see Fig. 11a) rather than a single minimum at the origin, as for  $t'/t < 1/2$ . This peculiar flatness of the spectrum leads to a square-root divergence of the density of states,  $\rho(\varepsilon) \propto \varepsilon^{-1/2}$  at the bottom of the band (Fig. 11b). Therefore in the low density limit (which is close to a vH band filling, since  $n_{vH} = 0$  for  $t'/t = 1/2$ ), saturated ferromagnetism is expected [23–25]. At  $t'/t = 1/2$  the  $T$ -matrix approximation [24] predicts rather high critical densities for the stability of ferromagnetism, e.g.  $n_c = 0.57$  for  $U = 4t$ . For  $t'/t = 0.45$  and  $U = 4t$  the same approach predicts ferromagnetism for densities  $0.3 < n < 0.5$ ; the smallest value of  $t'$  at which ferromagnetism can exist was predicted to be  $(t'/t)_c = 0.43$  for  $U = 4t$ . The projected QMC calculations [25] confirmed the existence of ferromagnetism for  $(t'/t)_c \gtrsim 0.47$ .

The phase diagram obtained within the TCRG approach for  $t'/t = 1/2$  is shown in Fig. 12. Similar to the antiferromagnetic instability, mean-field theory overestimates the tendency to magnetic order. The result of the  $T$ -matrix analysis of Ref. [24] for the critical concentration of the stability of ferromagnetism at  $U = 4t$  is marked by a cross. Surprisingly, this result is very close to the result of the RG approach. Similar to Ref. [47] one may introduce the quantity  $q_F(U) = n_c/n_c^{\text{MF}}$  to measure the deviation from the mean-field result at  $t'/t = 1/2$ . The analysis of the data shows that  $q_F(U)$  slightly increases with decreasing  $U$  and  $q_F(U \rightarrow 0) \simeq 0.8$ .

We have also explored the possibility for triplet ( $p$ -wave) pairing in the vicinity of the ferromagnetic phase. Although the  $p$ -wave pairing susceptibility is dominant in this region, a conclusive low-temperature extrapolation for the inverse susceptibility is not possible.

Therefore it is not clear whether a finite crossover temperature  $T_{\text{pSC}}^*$  exists. In any case the possible values for  $T_{\text{pSC}}^*$  must be significantly smaller than the crossover temperatures for  $d$ -wave superconductivity. The region where  $\ln(t/T_X) < 8$  is shown in Fig. 12, too. The growing of the vertices near the ferromagnetic phase results from the triplet  $p$ -wave superconducting fluctuations, but, unfortunately, the smallness of the temperature crossover scale, which is far below the range of applicability of the TCRG method prevents a safe conclusion about the possibility of a  $p$ -wave superconducting ground state.

Now we consider the case  $t'/t < 1/2$ , which is very different from the above-discussed case  $t'/t = 1/2$ . The square-root divergence of the density of states is replaced by a logarithmical divergence at the energy of the vHS,  $\rho(\varepsilon) \propto \ln(t/\varepsilon)$ , while the density of states is finite at the lower band edge (see Fig. 13). The phase diagram for  $t'/t = 0.45$  is presented in Fig. 14, where we again mark by cross the result of the  $T$ -matrix approximation. The ferromagnetic region substantially shrinks with decreasing  $t'$ : it reduces to a narrow density window around the vH band filling  $n_{VH} = 0.465$  (the corresponding critical densities are almost symmetrical around  $n_{VH}$  so that only the region  $n > n_{VH}$  is shown). Nevertheless, the ferromagnetic region is wider than in the  $T$ -matrix approximation. The same tendency is reflected in the RG result for the critical value  $(t'/t)_c \approx 0.3$  for the disappearance of ferromagnetism at  $U = 4t$ , which is much lower than the result of the  $T$ -matrix approximation cited above,  $(t'/t)_c = 0.43$ . As well as for the case  $t' = 1/2$  we also find an increasing triplet superconducting susceptibility away from the ferromagnetic phase, while the possible corresponding crossover temperatures  $T_{\text{pSC}}^*$  remain undetectably small.

#### IV. SUMMARY AND CONCLUSIONS

We have considered the phase diagrams of the  $t$ - $t'$  Hubbard model within two- and many-patch RG approaches as shown in Figs. 8, 9, 10, 12, and 14. Instabilities towards antiferro- or ferromagnetic order as well as to singlet  $d$ -wave superconductivity are identified in different parameter regimes. Near the ferromagnetic region the  $p$ -wave superconducting

susceptibility is enhanced, but a conclusion about a possible triplet superconducting ground state remains elusive.

At small  $t'$  and vH band fillings the antiferromagnetic instability dominates. With increasing  $t'$  antiferromagnetism is replaced by  $d$ -wave superconductivity. At larger  $t'/t$  ferromagnetism becomes the leading instability. The tendency towards  $d$ -wave superconductivity decreases with increasing  $U$  while antiferromagnetism is enhanced. We found that the two-patch approach predicts correctly the boundary of the ferromagnetic phase at vH band fillings, while it fails to reproduce correctly the boundary between antiferromagnetic and superconducting phases at small  $t'$  where nearly nesting effects become important.

Antiferromagnetism at small  $t'$  and ferromagnetism at  $t'/t = 1/2$  exist in broad density ranges around vH band fillings; the antiferromagnetism remains commensurate in the part of the phase diagram where the long-range ordered ground state is expected. The density ranges for magnetic order, found from TCRG are substantially narrower (2.5 times for the AF instability and 1.3 times for the F instability at small  $U$ ) than the corresponding mean-field results.

At half-filling at different  $t'$  we find the critical interaction strengths for the antiferromagnetic instability. From the present analysis we can not argue, whether the antiferromagnetic state we find is metallic or insulating. It was proposed [50] that at nonzero  $t'$  there is a finite interaction range  $U_c < U < U'_c$  for metallic antiferromagnetism, at  $U > U'_c$  it is replaced by the insulating AF state. On the other hand, the existence of a paramagnetic insulating state at larger  $t'$  was conjectured in Ref. [52]. Discriminating between these possibilities requires the calculation of the conductivity and the Drude weight, for which it is necessary to retain the frequency dependence of the vertices.

The boundary of ferromagnetism at  $t' = t/2$  found from TCRG is surprisingly close to the  $T$ -matrix approximation result in Ref. [24] at  $U = 4t$ , although the corresponding filling is not small and possibly outside the region of the validity of the  $T$ -matrix approximation. In the vicinity of antiferro- and ferromagnetic phases we found regions with enhanced  $d$ -wave and  $p$ -wave superconductivity, respectively. Not too close to the antiferromagnetic phase

the crossover temperatures for  $d$ -wave superconductivity into the corresponding renormalized classical regime with exponentially large correlation length can be estimated from the extrapolation to low temperatures of RG data for the order-parameter susceptibilities. At the same time, triplet  $p$ -wave superconductivity in the vicinity of the ferromagnetic phase possibly has much smaller crossover temperatures  $T_{\text{pSC}}^*$  which can not be determined safely from the present RG analysis.

The ferromagnetic phase substantially shrinks for  $t'/t < 1/2$  and the difference to the mean-field result increases. For this case, the  $T$ -matrix approach underestimates the tendency towards ferromagnetism. The tendency towards triplet  $p$ -wave superconductivity in the vicinity of the ferromagnetic phase persists, although its associated temperature crossover scale remains very low - significantly lower than for  $d$ -wave superconductivity.

It remains an open issue, how the above results change, when the two-loop corrections to the RG equations are taken into account, and how the electronic self-energy evolves in the vicinity of magnetic or superconducting instabilities. Another interesting issue for future work remains the question whether inhomogenous spin and charge structures are possible near half-filling and whether the Pomeranchuk instability may become the leading instability for anisotropic extensions of the 2D Hubbard model; if it does it is natural to connect this tendency to the stripe pattern formation in rare-earth doped  $\text{La}_{2-x}\text{Sr}_x\text{CuO}_4$ . Furthermore, the tendency towards  $p$ -wave superconductivity near the ferromagnetic phase of the  $t$ - $t'$  model suggests a possible route for future investigations of the origin of triplet pairing in  $\text{Sr}_2\text{RuO}_4$ .

## ACKNOWLEDGEMENTS

We are grateful to W. Metzner, G. Uhrig, and M. I. Katsnelson for insightful discussions. This work was supported by the Deutsche Forschungsgemeinschaft through SFB 484.

## APPENDIX. THE TEMPERATURE CROSSOVER TO THE RENORMALIZED CLASSICAL REGIME

In this Appendix we discuss how the temperature dependence of the magnetic susceptibilities changes at the crossover to the renormalized-classical regime. As a first example, we consider the 2D ferro- and antiferromagnetic Heisenberg models

$$H = \pm J \sum_{\langle ij \rangle} \mathbf{S}_i \cdot \mathbf{S}_j \quad (21)$$

(plus corresponds to the antiferro-, minus to the ferromagnet,  $J > 0$ ). The susceptibility (staggered susceptibility in the AF case) at high temperatures  $T \gg J$  obeys the Curie law

$$\chi_{\text{F,AF}} = \frac{C}{T} \quad (22)$$

where  $C = JS(S+1)/3$ . On the other hand, at temperatures  $T \ll J$  it was found from the RG analysis of the 2D nonlinear sigma model [41,42]

$$\chi_{\text{F,AF}} = C' \frac{T}{J^2} \xi^2 \quad (23)$$

where

$$\xi = C_\xi \begin{cases} \exp(2\pi\rho_s/T) & \text{AF} \\ (T/J)^{1/2} \exp(2\pi JS/T) & \text{F} \end{cases} \quad (24)$$

is the correlation length,  $C_\xi, C'$  are temperature-independent prefactors, and  $\rho_s$  is the zero-temperature value of the spin stiffness, which is proportional to the ground-state (sublattice) magnetization  $\bar{S}_0$ . Therefore, below the crossover temperature  $T^* \sim 2\pi J\bar{S}_0$  ( $\bar{S}_0 = S$  for a ferromagnet) the susceptibility becomes exponentially large.

Similar results can be obtained for the Hubbard model within the two-particle self-consistent approach [43]. We have

$$\chi_{\text{F,AF}} = \frac{\chi_{\mathbf{Q}}^0(T)}{1 - U_{sp}(T)\chi_{\mathbf{Q}}^0(T)} \quad (25)$$

where  $\mathbf{Q}=(\pi, \pi)$  in the AF case,  $\mathbf{Q}=\mathbf{0}$  in the F case, and  $\chi_{\mathbf{Q}}^0(T) = \chi_0(\mathbf{Q}, 0, T)$  is the zero-frequency limit of the bare dynamic susceptibility

$$\chi_0(\mathbf{q}, i\omega_n, T) = \sum_{\mathbf{k}} \frac{f_{\mathbf{k}} - f_{\mathbf{k}+\mathbf{q}}}{i\omega_n - \varepsilon_{\mathbf{k}} + \varepsilon_{\mathbf{k}+\mathbf{q}}}. \quad (26)$$

The effective interaction  $U_{sp}(T)$  satisfies the self-consistent equation

$$2n - n^2 \frac{U_{sp}(T)}{U} = 4T \sum_{\mathbf{q}, i\omega_n} \frac{\chi_0(\mathbf{q}, i\omega_n, T)}{1 - U_{sp}(T)\chi_0(\mathbf{q}, i\omega_n, T)}. \quad (27)$$

At high temperatures  $T \gg t$  we have  $U_{sp}(T) \simeq U$  and

$$\chi_{F,AF} \simeq \chi_{\mathbf{Q}}^0(T) \simeq \frac{1}{4T}. \quad (28)$$

At small temperatures the denominator in Eq. (27) can be expanded for wavevectors  $\mathbf{q}$  close to  $\mathbf{Q}$  (cf. Ref. [43]) and one obtains

$$\bar{\sigma}_0^2 = \frac{2T\chi_0}{AN} \sum_{\mathbf{q}} \frac{1}{\xi^{-2} + (\mathbf{q} - \mathbf{Q})^2} \quad (29)$$

where  $\chi_0 = \chi_0(\mathbf{Q}, 0, 0)$ ,  $A = \nabla^2 \chi_0(\mathbf{q}, 0, 0)|_{\mathbf{q}=\mathbf{Q}}$ , and  $\bar{\sigma}_0^2 = n - n^2 U_{sp}(0)/2 - \mathcal{P}/2$  ( $\mathcal{P}$  is the zero-temperature value of the r.h.s. of Eq. (27)), and  $\xi^{-2} = [1 - U_{sp}(T)\chi_0(\mathbf{Q}, 0, T)]/A$ . Momentum integration in Eq. (29) leads to

$$\xi = C_\xi \exp\{nA\bar{\sigma}_0^2/2T\chi_0\} \quad (30)$$

and

$$\chi_{F,AF} = \chi_0 \xi^2.$$

In this case the crossover temperatures  $T_{F,AF}^* \sim t\bar{\sigma}_0^2$ . Therefore these examples show that

$$\chi_{F,AF} = \begin{cases} C/T & T \gg T^* \\ C'\xi^2 & T \ll T^* \end{cases}$$

and the correlation length  $\xi \propto \exp(\mathcal{A}T^*/T)$  is exponentially large in the low-temperature, renormalized classical regime.

## REFERENCES

- [1] D. J. Scalapino, Phys. Rep. **251**, 1 (1994); J. Low Temp. Phys. **117**, 179 (1999).
- [2] N. E. Bickers, D. J. Scalapino, and S. R. White, Phys. Rev. Lett. **62**, 961 (1989).
- [3] S. C. Zhang, Science **275**, 1089 (1997); E. Demler and S. C. Zhang, Nature (London) **396**, 733 (1998).
- [4] J. Schmalian, D. Pines, and B. Stojkovic, Phys. Rev. Lett. **80**, 3839 (1998).
- [5] A. Chubukov, D. Pines, and B. Stojkovic, J. Phys.: Condens. Matter **8**, 10017 (1996);  
A. Chubukov and D. Morr, Phys. Rep. **288**, 355 (1997); A. Abanov and A. Chubukov,  
Phys. Rev. Lett. **84**, 5608 (2000).
- [6] Y. Maeno, T. M. Rice, and M. Sigrist, Physics Today **54**, 42 (2001).
- [7] I. I. Mazin and D. J. Singh, Phys. Rev. Lett. **79**, 733 (1997); *ibid.* **82**, 4324 (1999).
- [8] S. Murakami, N. Nagaosa, and M. Sigrist, Phys. Rev. Lett. **82**, 2939 (1999).
- [9] Y. Sidis, M. Braden, P. Bourges, B. Hennion, S. Nishizaki, Y. Maeno, and Y. Mori,  
Phys. Rev. Lett. **83**, 3320 (1999).
- [10] N. Kikugawa and Y. Maeno, cond-mat/0211248 (unpublished).
- [11] F. Nakamura, T. Goko, M. Ito, T. Fujita, S. Nakatsuji, H. Fukazawa, Y. Maeno, P.  
Alireza, D. Forsythe, and S. R. Julian, Phys. Rev. B **65**, 220402(R) (2002).
- [12] A. Ino, C. Kim, M. Nakamura, T. Yoshida, T. Mizokawa, A. Fujimori, Z.-X. Shen, T.  
Kakeshita, H. Eisaki, and S. Uchida, Phys. Rev. B **65**, 094504 (2002).
- [13] P.V. Bogdanov, A. Lanzara, X.J. Zhou, S.A. Kellar, D.L. Feng, E.D. Lu, H. Eisaki, J.-I.  
Shimoyama, K. Kishio, Z. Hussain, and Z. X. Shen, Phys. Rev. B **64**, 180505 (2001).
- [14] D.L. Feng, C. Kim, H. Eisaki, D.H. Lu, A. Damascelli, K.M. Shen, F. Ronning, N.P.  
Armitage, N. Kaneko, M. Greven, J. Shimoyama, K. Kishio, R. Yoshizaki, G.D. Gu,

- and Z.-X. Shen, Phys. Rev. B **65**, 220501(R) (2002).
- [15] A. Damascelli, D. H. Lu, K. M. Shen, N. P. Armitage, F. Ronning, D. L. Feng, C. Kim, Z.-X. Shen, T. Kimura, Y. Tokura, T. Tsukuba, Q. Mao, and Y. Maeno, Phys. Rev. Lett. **85**, 5194 (2000).
- [16] T. Tohyama and S. Maekawa, Supercond. Sci. Tech. **13**, R17 (2000).
- [17] T. Oguchi, Phys. Rev. B **51**, 1385 (1995); D. J. Singh, Phys. Rev. B **52**, 1358 (1995).
- [18] D. F. Agterberg, T. M. Rice, and M. Sigrist, Phys. Rev. Lett. **78**, 3374 (1997).
- [19] H. Q. Lin and J. E. Hirsch, Phys. Rev. B **35**, 3359 (1987)
- [20] R. R. Santos, Phys. Rev. B **39**, 7259 (1989).
- [21] B. Normand and A. P. Kampf, Phys. Rev. B **65**, 020509 (2002).
- [22] H. Tasaki, Phys. Rev. Lett. **69**, 1608 (1992); A. Mielke and H. Tasaki, Commun. Math. Phys. **158**, 341 (1993).
- [23] M. Fleck, A. Oles, and L. Hedin, Phys. Rev. B **56**, 3159 (1997).
- [24] R. Hlubina, Phys. Rev. B **59**, 9600 (1999)
- [25] R. Hlubina, S. Sorella, and F. Guinea, Phys. Rev. Lett. **78**, 1343 (1997).
- [26] D. Zanchi and H.J. Schulz, Phys. Rev. B **54**, 9509 (1996); *ibid.* **61**, 13609 (2000).
- [27] C. J. Halboth and W. Metzner, Phys. Rev. B **61**, 7364 (2000).
- [28] C. Honerkamp, M. Salmhofer, N. Furukawa, and T.M. Rice, Phys. Rev. B **63**, 035109 (2001).
- [29] V. Yu. Irkhin, A. A. Katanin, and M. I. Katsnelson, Phys. Rev. B **64**, 165107 (2001).
- [30] C. Honerkamp and M. Salmhofer, Phys. Rev. B **64**, 184516 (2001).
- [31] J. V. Alvarez, J. Gonzalez, F. Guinea, and M. A. H. Vozmediano, J. Phys. Soc. Jpn,



- 67**, 1868 (1998); cond-mat/9804153 (unpublished); F. Guinea, Nucl. Phys. B **642**, 407 (2002).
- [32] J. Kanamori, Progr. Theor. Phys. **30**, 275 (1963).
- [33] C. J. Halboth and W. Metzner, Phys. Rev. Lett. **85**, 5162 (2000).
- [34] C. Honerkamp, M. Salmhofer, and T. M. Rice, Eur. Phys. J. B **27**, 127 (2002).
- [35] R. Shankar, Rev. Mod. Phys. **66**, 129 (1994).
- [36] P. Lederer, G. Montambaux, and D. Poilblanc, J. Phys. (Paris) **48**, 1613 (1987).
- [37] N. Furukawa, T. M. Rice, and M. Salmhofer, Phys. Rev. Lett. **81**, 3195 (1998).
- [38] A. P. Kampf and A. A. Katanin, Phys. Rev. B **67**, 125104 (2003).
- [39] K. G. Wilson and J. Kogut, Phys. Rep. **12**, 77 (1974).
- [40] B. Binz, D. Baeriswyl, and B. Doucot, Eur. Phys. J. B **25**, 69 (2002).
- [41] S. Chakravarty, B. I. Halperin, and D. R. Nelson, Phys. Rev. B **39**, 2344 (1989).
- [42] P. Kopietz and S. Chakravarty Phys. Rev. B **40**, 4858 (1989)
- [43] A. M. Dare, Y. M. Vilk, and A. M. S. Tremblay, Phys. Rev. B **53**, 14236 (1996); Y. M. Vilk and A. M. S. Tremblay, J. Phys. I (France) **7**, 1309 (1997).
- [44] V. L. Berezinskii, ZhETF **59**, 907 (1970) [Sov. Phys. JETP **32**, 493 (1970)]; L. M. Kosterlitz and D. J. Thouless, J. Phys. C **6**, 1181 (1973).
- [45] J. B. Kogut, Rev. Mod. Phys. **51**, 659 (1979).
- [46] We determine the leading order parameter by the highest value of the crossover temperature  $T_m^*$  found from the extrapolation of the inverse susceptibility, as described in Sect. IIB.
- [47] P. G. J. van Dongen, Phys. Rev. B **54**, 1584 (1996).

- [48] E. Dagotto, J. Riera, Y. C. Chen, A. Moreo, A. Nazarenko, F. Alcaraz, and F. Ortolani, Phys. Rev. B **49**, 3548 (1994); F. Guinea, G. Gomez-Santos, and D. P. Arovas, Phys. Rev. B **62**, 391 (2000).
- [49] H. Kondo and T. Moriya, J. Phys. Soc. Jpn. **65**, 2559 (1996).
- [50] D. Duffy and A. Moreo, Phys. Rev. B **55**, R676 (1997).
- [51] W. Hofstetter and D. Vollhardt, Ann. Physik **7**, 48 (1998).
- [52] T. Kashima and M. Imada, J. Phys. Soc. Jpn. **70**, 3052 (2001).

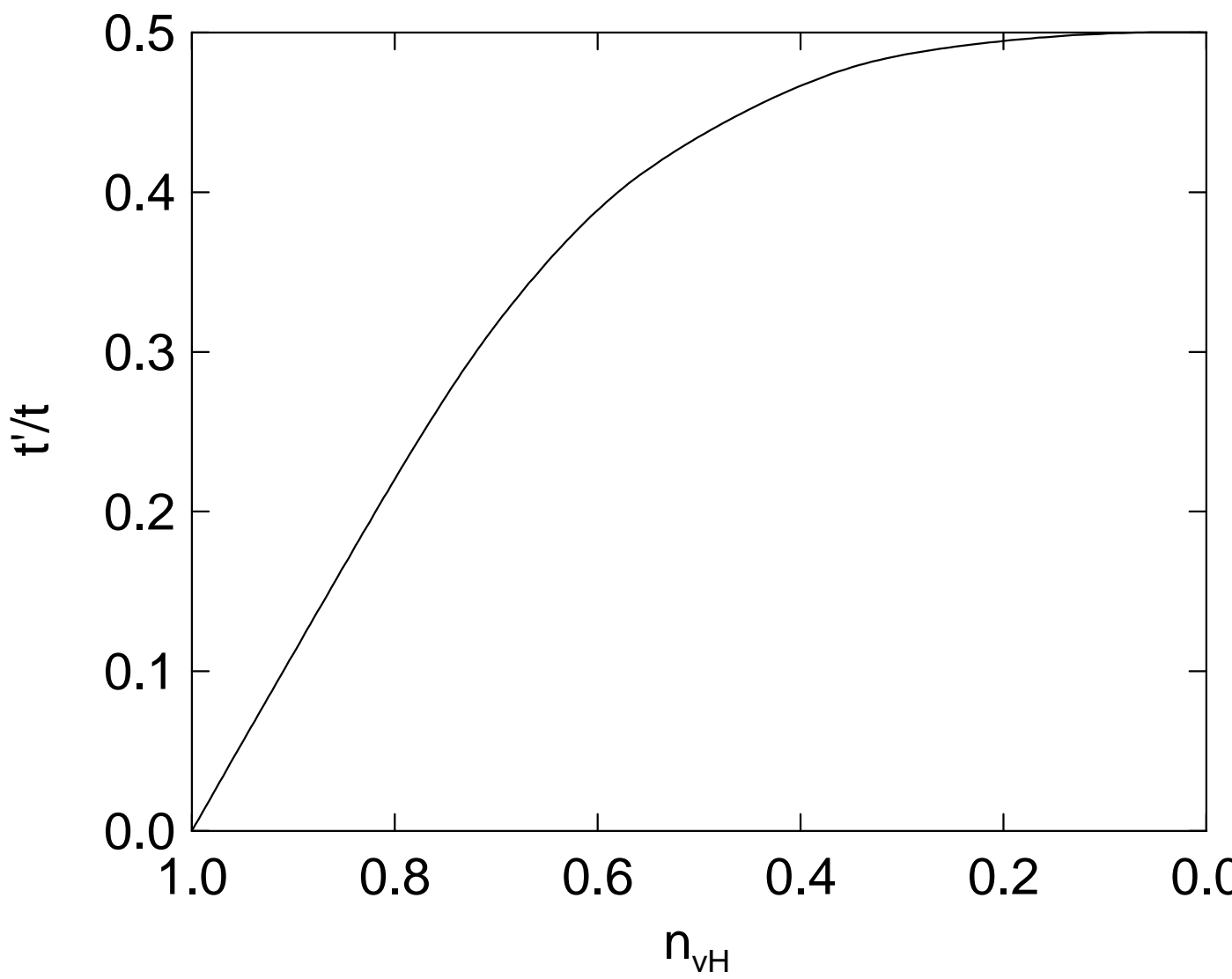
## FIGURE CAPTIONS

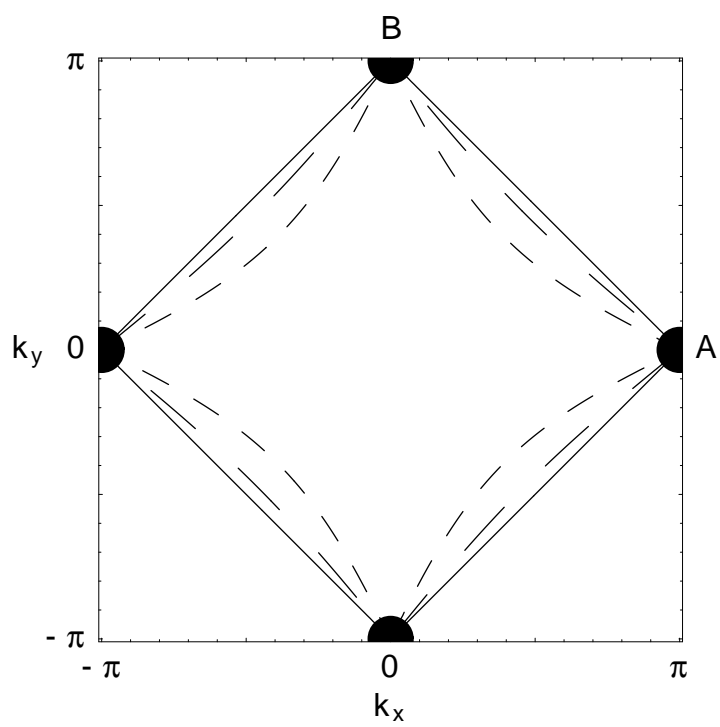
1. The dependence of the van Hove band filling on  $t'/t$ .
2. The Fermi surface at van Hove band fillings:  $t' = 0$  and  $n = 1$  (solid line),  $t'/t = 0.1$  and  $n = 0.92$  (long-dashed line), and  $t'/t = 0.3$  and  $n = 0.72$  (short-dashed line),  $A$  and  $B$  are van Hove points.
3. The division of momentum space into patches in the two-patch approach. Regions I contain the momenta closest to the vH singularity points  $\mathbf{k}_A$  and  $\mathbf{k}_B$ , regions II contain the momenta which are close to the FS but far from vH singularities and regions III contain the momenta far from both, FS and vH singularities.
4. The four types of vertices considered in the two-patch approach: (a) and (b) correspond to exchange and direct scattering between different vH singularities respectively, (c) umklapp scattering, (d) intrapatch scattering. The incoming and outgoing momenta with equal spin are connected by solid lines inside the vertices.
5. a) Scaling behavior of the coupling constants at  $t'/t = 0.1$ . The solid line corresponds to  $g_1$ , dashed line to  $g_2$ , dash-dotted line to  $g_3$ , dotted line to  $g_4$ . b) Scaling behavior of the susceptibilities at  $t'/t = 0.1$ . Solid line corresponds to the AF, dashed line to the dSC, and dotted line to the F susceptibility. The interaction strength is  $U = 2t$ .
6. The same as in Fig. 5 for  $t'/t = 0.45$ .
7. Diagrammatic representation for the many-patch RG equations, Eq. (15). Lines drawn through the vertices show the direction of spin conservation. Diagrams are drawn in the same order as the respective terms in Eq. (15). The cutting dash at the propagator lines means the derivative with respect to  $T$  (for brevity we indicate only the derivative of one of the propagators, the same diagrams with derivatives of another propagator are included as well).

8. Phase diagram at vH band fillings as obtained from two- and many-patch RG analyses. Solid lines correspond to the phase boundaries obtained within the two-patch RG analysis. The symbols show the results of the many-patch RG approach: closed circles correspond to AF, open circles to incommensurate  $(\pi, \pi - \delta)$  order, diamonds to dSC, and triangles to the F phase. Long-dashed line is the boundary of ferromagnetic phase obtained in Ref. [31] (see text).
9. Phase diagram for  $t' = 0$ . The dashed line is the mean-field phase boundary between antiferromagnetic and paramagnetic phases, the solid line is the boundary of the antiferromagnetic phase obtained from the temperature-cutoff many-patch RG approach. The corresponding result of Ref. [27] for the boundary of the antiferromagnetic phase is shown by dotted line. The dot-dashed, dot-dot-dashed, and dot-dot-dot-dashed lines are contour lines for the  $d$ -wave superconducting crossover temperature into renormalized classical regime  $T_{\text{dSC}}^* = e^{-5}t, e^{-6}t$ , and  $e^{-7}t$  respectively (see text). The inset shows the phase diagram in  $\mu$ - $U$  coordinates.
10. Phase diagram at  $n = 1$  (half-filled case). The notations are the same as in Fig. 9. The cross corresponds to the critical  $U_c$  for the stability of the antiferromagnetic phase at  $t'/t = 0.2$  as obtained from QMC calculations [19], the star marks the result of the path-integral RG approach for  $U_c$  [52].
11. The electronic dispersion (a) and non-interacting density of states (b) at  $t'/t = 1/2$ .
12. The phase diagram for  $t'/t = 1/2$ . The long-dashed line MF(F) is the mean-field phase boundary between ferromagnetic and paramagnetic phases, the dot-dashed line MF(S) is the mean-field result for the boundary of saturated ferromagnetism. The solid line is the boundary of ferromagnetic phase obtained from the temperature-cutoff many-patch RG approach, the short-dashed line is the contour line above which the maximal vertex reach  $V_{\text{max}} = 18t$  at the temperature  $T_X > e^{-8}t$ . The  $T$ -matrix phase boundary for the ferromagnetic phase [24] at  $U = 4t$  is marked by cross. The inset shows the phase

diagram in  $\mu$ - $U$  coordinates., pSC marks the region where the triplet superconducting susceptibility is dominating.

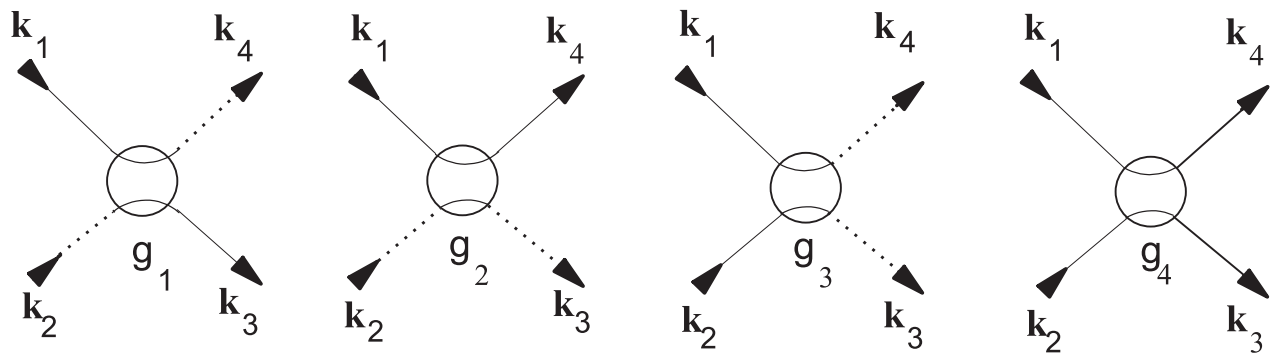
13. The non-interacting density of states for  $t' = 0.45t$ .
14. The phase diagram for  $t'/t = 0.45$ . The notations are the same as in Fig. 12.

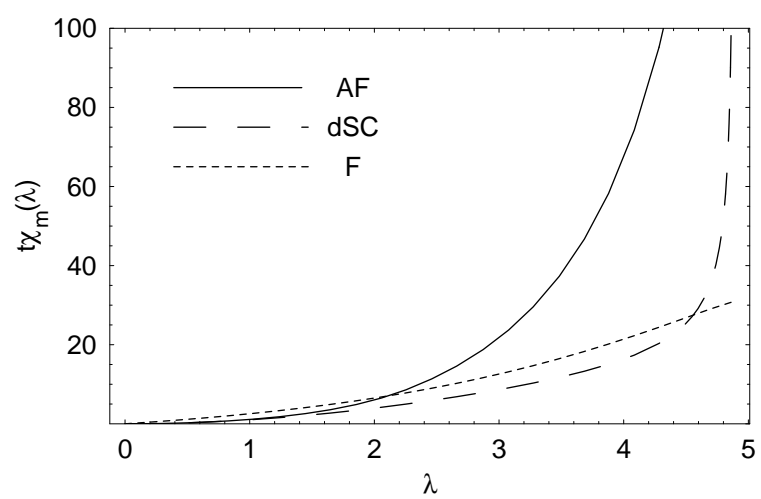
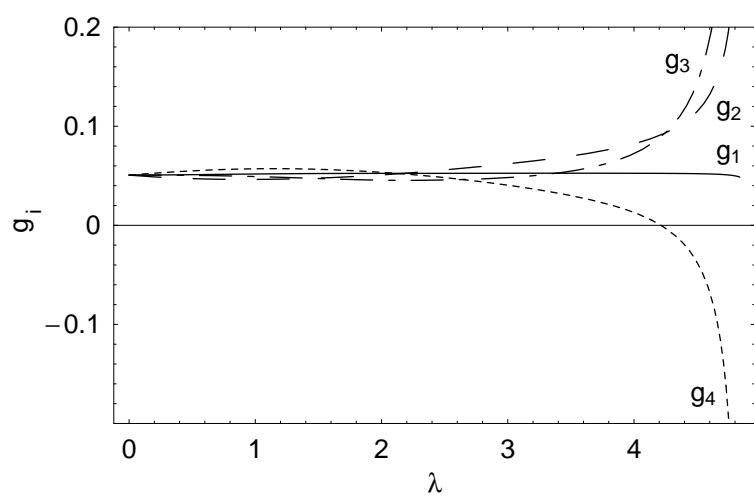


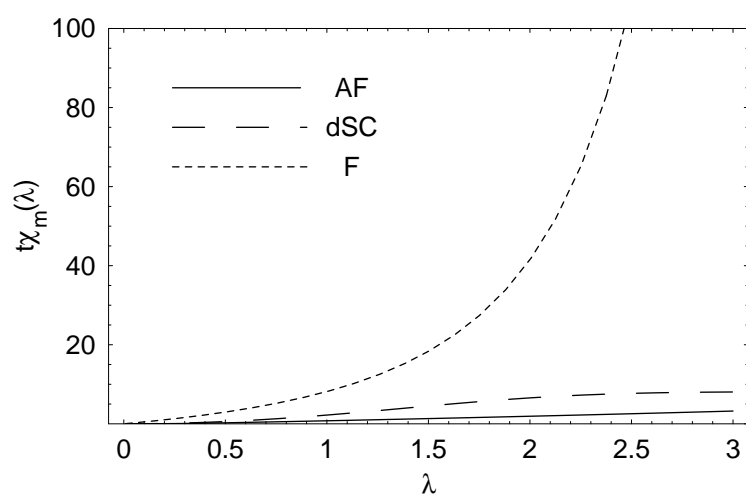
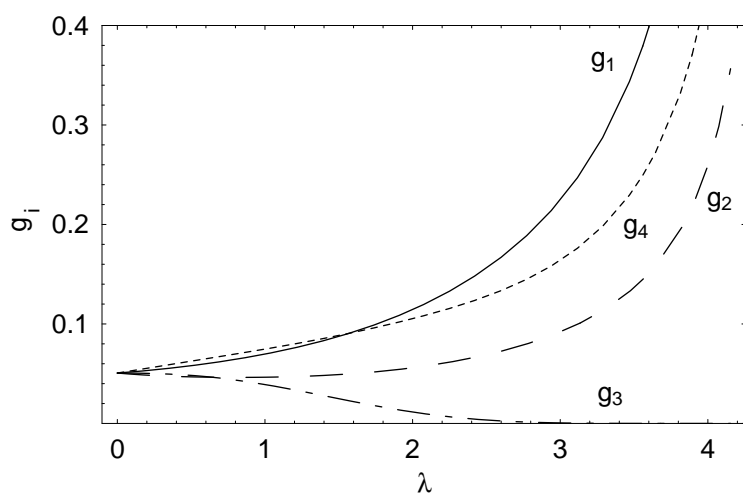












$$\begin{aligned}
 \frac{d}{dT} \left( \text{Diagram 1} \right) &= \text{Diagram 2} + \\
 &+ \text{Diagram 3} + \text{Diagram 4} + \text{Diagram 5} + \text{Diagram 6}
 \end{aligned}$$

The diagrams are Feynman-like diagrams with four external lines labeled  $k_1, k_2, k_3, k_4$ .  
 - **Diagram 1:** A circle with four external lines meeting at a single point. Arrows point outwards:  $k_1$  (top-left),  $k_3$  (top-right),  $k_2$  (bottom-left), and  $k_4$  (bottom-right).  
 - **Diagram 2:** Two circles connected by two horizontal lines. The left circle has external lines  $k_1$  and  $k_2$ ; the right circle has  $k_3$  and  $k_4$ . The connecting lines have arrows pointing right, with a slash on the top line.  
 - **Diagram 3:** Two circles connected by two vertical lines. The left circle has external lines  $k_1$  and  $k_2$ ; the right circle has  $k_3$  and  $k_4$ . The connecting lines have arrows pointing up, with a slash on the right line.  
 - **Diagram 4:** Two circles connected by two horizontal lines. The left circle has external lines  $k_1$  and  $k_2$ ; the right circle has  $k_3$  and  $k_4$ . The connecting lines have arrows pointing right, with a slash on the top line.  
 - **Diagram 5:** Two circles connected by two vertical lines. The left circle has external lines  $k_1$  and  $k_2$ ; the right circle has  $k_3$  and  $k_4$ . The connecting lines have arrows pointing up, with a slash on the right line.  
 - **Diagram 6:** Two circles connected by two horizontal lines. The left circle has external lines  $k_1$  and  $k_2$ ; the right circle has  $k_3$  and  $k_4$ . The connecting lines have arrows pointing right, with a slash on the top line.

